

# Exploratory Projection to Latent Structure Models for use in Transcriptomic Analysis

Edward Tjörnhammar<sup>†,‡</sup> and Richard Tjörnhammar<sup>\*</sup>

<sup>†</sup>KTH Royal Institute of Technology, SE-100 44 Stockholm, Sweden

<sup>‡</sup>FOI Swedish Defence Research Agency, SE-164 90 Stockholm, Sweden

<sup>\*</sup>KI Karolinska Institutet, SE-171 71 Stockholm, Sweden

March 18, 2021

## Abstract

In this paper, we ask if it is possible to increase the interpretability in multivariate analysis by aligning and projecting covariates onto comparative subspaces. We demonstrate our method as well as the interpretative power of Partial Least Squares (PLS) decomposed models and how robust interpretability can lead to quantitative insights.

We discuss the statistical properties of the PLS weights,  $p$ -values associated with specific axes, as well as their alignment properties.

The applicability of this approach within life science is also demonstrated by applying it to three use cases of publically available datasets.

Further we present hierarchical pathway enrichment results stemming from aligned  $p$ -values, which are compared with results derived from enrichment analysis, as an external validation of our method.

We find that the method can uncover known results from genomics for all of the studied use cases, i.e. microarray data from multiple sclerosis and diabetes patients as well as RNA sequencing data from breast cancer patients.

**Keywords**— Orthogonal Projections to Latent Structures, Statistical Methodology, Dimensionality Reduction Analysis, Descriptive Statistics, Bioinformatics

## 1 Introduction

Many fields within Life Science, such as transcriptomics (the study of transcripts), proteomics (the study of proteins), or metabolomics (the study of metabolites) characteristically rely upon datasets which has “few samples” but “many features”. One is furthermore typically interested in discovering which collection of analytes are modulating specific attributes.

Orthogonal Projection to Latent Structures (OPLS) models [1, 2] have a long history of usage in metabolomics [3, 4], as well as other fields of research. The ability to decompose and align the feature space while communicating the effect of the decomposition on sample space is a well-known property of OPLS models. The OPLS methods have long been employed for characterisation of data features, but the interpretation often stops once the sample and feature groupings have been identified.

Both Principle Component Analysis (PCA) [5] and OPLS create new predictor variables often termed components. The components created by PCA maximize the variance in each without regard for the response. In PCA, we get a large number of components that aim to describe orthogonal variance. This affine transform can be further exploited to evaluate the statistical significance of weight relations. Similar to PCA, the OPLS decomposes an input matrix into unique and complementary matrices. However, unlike PCA, which ultimately relies on factorising a sample centred expression matrix along the components of maximal orthogonal variance, the OPLS method instead decomposes an input matrix by maximizing the mutual covariance between the feature space projection against the sample space response projection on the OPLS predictor plane.

The subspace plane could be any dimensionality and in PLS regression the NIPALS algorithm ensures that the covariance between the score and weight vectors are aligned. [6] (second equation). Because the weights are commonly computed via an iterative procedure it does not necessarily converge to a good solution, it however often does. Once the solution has been obtained then the variance in the dataset is often better described by fewer components than in PCA. It is not strange because the goal is to model the response by directly decomposing variance onto components describing the response. For this reason, a OPLS algorithm is similar to a two-way linear regression ANalysis Of VAriance (ANOVA) [7]. In both methods a two-dimensional tensor is constructed to describe the response and as such both methods are prone to similar issues and produce similar statistical insights. We will see that, as opposed to a two-way ANOVA model, the OPLS model also divulge information about the directionality of the variation along an axis.

In [8] the authors make a point that OPLS regression coefficients used in ranked analysis do not take advantage of the multivariate nature of OPLS. This holds even for our work, we project the decomposition down onto a univariate vector to increase the robustness of our model interpretations.

We define a pathway as a knowledge-based group descriptor of the transcripts. It should not be confused with the path diagram of the latent variables [2]. Connecting the weights with axis  $p$ -values and calculating pathway enrichment becomes an important sanity check for this method. There are several knowledge-based pathway databases [9, 10, 11, 12]. These are curated with regards to known activity of transcripts and as such are not deduced from knowledge inherent in the data. In theory a new and properly well carried out experiment should be unknown to the knowledge database curator facilitating the group definitions. As such, if the alignment of weights to a descriptor axis is sensible then, the pathway enrichments should convey sensible enrichment for the groups that are under study.

For our purposes; Given the feature and sample space description matrices ( $\mathbf{X}$ ,  $\mathbf{Y}$ ) are described by their corresponding weights ( $\mathbf{W}$ ,  $\mathbf{C}$ ) and scores ( $\mathbf{T} = \mathbf{XW}$ ,  $\mathbf{U} = \mathbf{YC}$ ). If the PLS algorithm has converged on a solution, by maximizing covariance between  $\mathbf{T}$  and  $\mathbf{U}$ , then  $\mathbf{w}$  and  $\mathbf{c}$  will be aligned on the projected subspace [6].

In this work we propose a method for decision research support in noisy domains. We believe it to be able to find plausible research targets by an exploration of the

feature space encoding in high entropy domains through comparative plotting of cosine alignment on PLS decomposition. This method is similar to OPLS [13], but it does not perform discriminant analysis, such as in OPLS-DA, which facilitates the analysis of categorical data. Using this approach, with encoded information and utilizing the  $\mathbf{C}$  space as an attribute compass in the feature weight plane one is able to compute  $p$ -values for sample attributes in a PLS context.

As such we demonstrate that the alignment PLS decomposition can be directly utilized for  $p$ -value calculations. We also demonstrate that large values along the attribute axis corresponds to large fold change contribution between groups along said axis.

We believe the main contributions of the paper to be:

- An exploratory technique combining alignment and angular representation of samples with regards to some distance measure. The exploratory PLS method creates a robust multidimensional fit whereby signal artifacts not aligned with the encoding obtain small weights in their component.
- An evaluation of the method with regards to comparable analyses, i.e. T-test, ANOVA and PCA, as well as independent boxplot validation.
- A demonstration of said method with regards to already known results.
- A multivariate regression method implemented in python.

The remainder of the paper is structured as follows. Section 2 motivates and describes the statistical viewpoint and exemplifies analysis usage. A number of illustrating analysis examples related to the previously described method process are then presented in Section 3 in order to exemplify and validate the proposed solution. For validation purposes a comparison to t-testing is performed. Finally, Sections 4 and 5 provide an assessment analysis and conclude from the undertaken experiments.

## 2 Method

For our adaptation of the PLS method, Exploratory Projection to Latent Structures (EPLS), we employ the same nomenclature as in the work by [6]. We present an overview of the method in Figure 1.

It should be noted that the journal  $J$  and “analytes”  $A$  are respectively previously denoted  $X$  and  $Y$  in regular PLS. The journal  $J$  is simply named in this way since it is a record of the different patients and their biometrics.

We begin by specifying the encoding formula for the problem at hand. A formula is on the form:

$$y \sim C(x_1) : C(x_2) + C(x_3) + x_4$$

Meaning that  $y$  is inspected by encoding an  $X$  matrix constituting of the values of  $x_4$  from  $J$ , the binary class expansion of  $x_3$  from  $J$  and a binary class expansion of the binomial pair combinations of  $x_1$  and  $x_2$  from  $J$ . With a binary class expansion we mean that  $C$  encodes patient  $p$  “diabetic” biometric marker status as 1 or 0. As a concrete example we might have the patient journal as in Table 1. Which according formula, assuming  $x_1 = \text{Diabetic}$ ,  $x_2 = \text{Smoker} \dots$ , would encode into Table 2

As one can discern from Table 2 that the attributes are exploded into their value form and multi-class attributes, i.e. Diabetic here, compounded with the other attribute’s value form.

Diabetic	F	T <sub>2</sub>	T <sub>1</sub>	F
Smoker	S	S	F	F
Unemployed	F	S	F	F
Blood-sugar	0.5	5	4.1	0.1

Table 1: Example patient *Journal*

Given the subspace vectors  $\mathbf{W} \wedge \mathbf{T}$  we assume that any symmetry operations on  $\mathbf{W}$  will commute to  $\mathbf{T}$ . Habitually for our numerical experiments, we treat a set of gene expressions as the feature matrix  $\mathbf{X}$  and the patient journal, with coarse-grained end states, as the sample response matrix  $\mathbf{Y}$ . As such  $\mathbf{X}$  either represent a microarray- or a Fragments Per Kilobase of transcript per Million mapped reads (FPKM) Ribonucleic Acid (RNA)-sequence matrix.

The formulation of groups is done by retrieving journal value entries for a group present in the statistical formula enclosed with parentheses and a leading ‘*C*’. Example:

$$\text{Transcript} \sim C(\text{Group})$$

would retrieve the **Group** journal value entries.

To elaborate, the formula describes the

Since PLS2 maximizes the pairwise covariance score, feature weights and sample weights are “co-linearized” in a similar way. This lets us ascribe features to sample weights, one way is to employ tessellation. Each transcript is simply associated with the closest “formulae encoded axis”. The formulae encoded axes are defined by the PLS regression weights, using the above notation, of the  $Y$  matrix. We will refer to this target space as the “sample axis”. We haven’t proved this property since it is assured by the PLS regression work by [6].

For proximity we can either use absolute coordinate proximity on the weight projection plane or the angular proximity between the transcript and attribute axis weight. The formula for calculating the coordinate proximity follows  $1 - NN$  where the centroids are taken from the PLS  $\mathbf{Y}$  estimation  $\mathbf{C}$ . The formula for calculating the angular distance is given by the cosine similarity:

$$d = 1 - \cos(\alpha) = 1 - \frac{\mathbf{a} \cdot \mathbf{b}}{\|\mathbf{a}\| \cdot \|\mathbf{b}\|}$$

Here  $\mathbf{a}$ , a vector, designates a transcript weight position and  $\mathbf{b}$  a sample score weight position, also a vector. The angle  $\alpha$  is the angle between  $\mathbf{a}$  and  $\mathbf{b}$ . In summary, we perform the steps:

Diabetic.T <sub>1</sub> -Smoker.F	0	0	1	0
Diabetic.T <sub>2</sub> -Smoker.S	0	1	0	0
Diabetic.F-Smoker.F	0	0	0	1
Diabetic.F-Smoker.S	1	0	0	0
Unemployed.F	1	0	1	1
Unemployed.S	0	1	0	0
Blood-sugar	0.5	5	4.1	0.1

Table 2: Coded patient Table 1 *Journal*

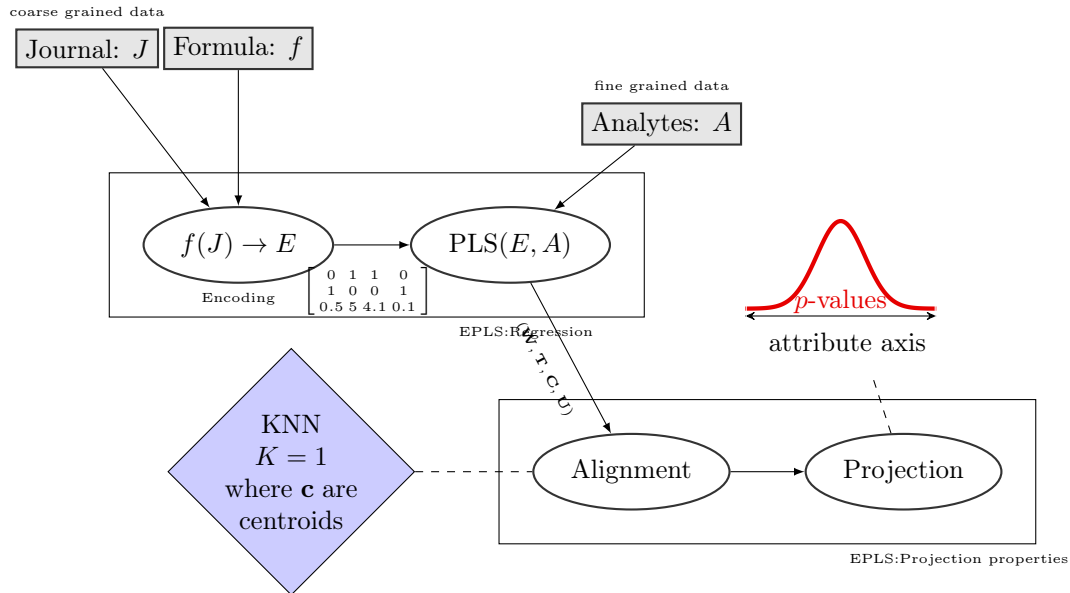


Figure 1: Method simplified workflow

1. Use a statistical test formula that defines the group variations to test, i.e.  $f$ .
2. Device an encoding data frame  $\mathbf{E}$  from journal group descriptor  $\mathbf{J}$  instances, i.e.  $f(\mathbf{J}) \rightarrow \mathbf{E}$ .
3. Utilize PLS2 to find the solution to the formula using the expression matrix and patient (sample response) journal, i.e.  $PLS(\mathbf{E}, \mathbf{A}) \rightarrow (\mathbf{W}, \mathbf{T}, \mathbf{C}, \mathbf{U})$
4. Categorical membership is determined through either tessellation (euclidean distance) or angle, cosine distance (1-NN) to a centroid, the centroids are given by  $\mathbf{c}$ , which denotes a vector belonging to  $\mathbf{C}$ .
5. Calculate characteristic length scales of the prediction plane by finding the maximum weights for normalization purposes across the PLS components.
6. Calculate the projected density of the weights onto the group axes as encoded by the statistical test formula, i.e.  $\forall \mathbf{c} \in \mathbf{C} \wedge \mathbf{w} \in \mathbf{W}$  we calculate the projections  $r = \frac{\mathbf{c} \cdot \mathbf{w}}{\|\mathbf{c}\|}$
7. Calculate  $p$ -values for the projections belonging to a  $\mathbf{c}$  by assuming that the weights are distributed normally, using the complementary cumulative distribution function for the observed projection,  $Q(r) = 1 - \frac{1}{2} \left[ 1 + \operatorname{erf}\left(\frac{r-\mu}{\sigma\sqrt{2}}\right) \right]$ .
8. Calculate the ranking of the weights on the projected axis, mapped in ascending order from zero to one, i.e.  $\#\{i : |r_i| \leq r_j, \forall (i, j) \in \mathbf{c}\}$

This can be relied upon to visualize how features associate with samples.

Since ReactomePA [11] knowledge base is hierarchical, we also employed a hierarchical enrichment and correction scheme similar to the elim algorithm as suggested by [14].

## 2.1 Implementation

We have chosen to employ the PLS2 algorithm as implemented in the publicly available python [15] package and it also exists as an R [16, 17] package.

All categoricals present in the patient journal are translated into a binary encoding matrix. Thus all and any unique descriptors included in the group under study gets translated into a unique axis. All formula entries that are not categoricals are treated as real variables. The exact routine execution, visualization and calibration is covered in the experiment code [18].

The quantitative analysis relies on projecting the feature weight distribution onto an axis and studying the point density distribution on that axis. The  $p$  values are calculated from the cumulative error function for the density along the projection axis, see supplementary code [19]. The two-way ANOVA comparison is performed using the statsmodels [20] SciPy package.

## 3 Results

According to the method described in Section 2 we conducted three experiments:

- Multiple Sclerosis (MS) microarray dataset analysis, testing sample variation to group interaction. Also presenting the alignment properties of angular EPLS model interpretation.
- The Cancer Genome Atlas (TCGA)-Breast CAncer Gene (BRCA) two-way ANOVA, deducing the interaction model from the EPLS plot. Also comparing the analytical strength to type-2 ANOVA.
- Diabetes MICROARRAY dataset compounded analysis with clustering enrichment for genomic impact in Type 2 Diabetes (T2D).

The datasets for the analysis, as well as the group definition files, can all be found online [19]. Details of the processing of the MS, as well as TCGA dataset, is also deposited online [21].

### 3.1 Multiple Sclerosis and the alignment properties of EPLS models

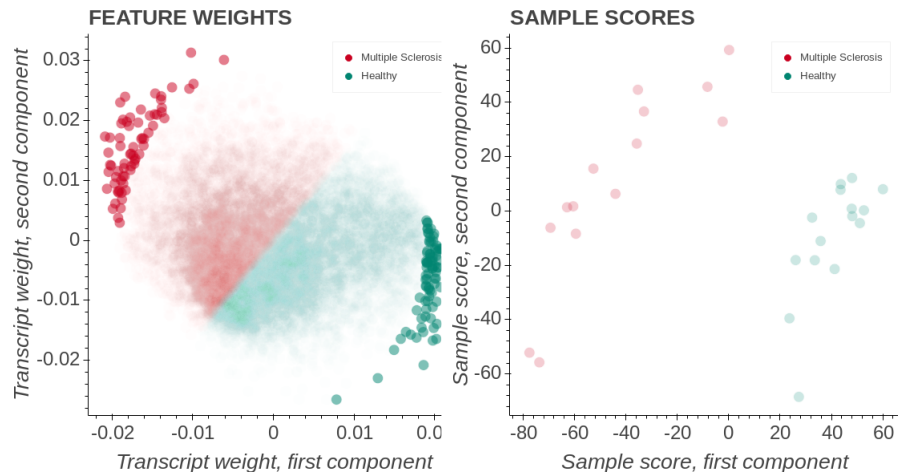
The Multiple Sclerosis microarray data was obtained via the Gene Expression Omnibus (GEO) accession number for the microarray dataset GSE21942<sup>1</sup>. 15 ‘Healthy’ controls and 14 ‘MS’ patients were processed and used in the analysis [22]. The EPLS model is conducting the test whether a transcript sample variation is well described by the between-group variation. We choose to express this as a statistical formula on the form

$$\text{Transcript} \sim C(\text{Status})$$

Here the **Status** label can take on the values **Healthy** or **MS**.

In Figure 2a we can see how the transcripts become aligned to the disease state. A large number of transcripts are positioned close to origo and those that are farther away than 99% of all transcripts are highlighted with a higher opacity. From Figure 2b, it is clear that the EPLS model separates the cohort well. By comparing the left and right graph we see that the transcript weights are aligned so that we only have

<sup>1</sup><http://www.ncbi.nlm.nih.gov/geo/>



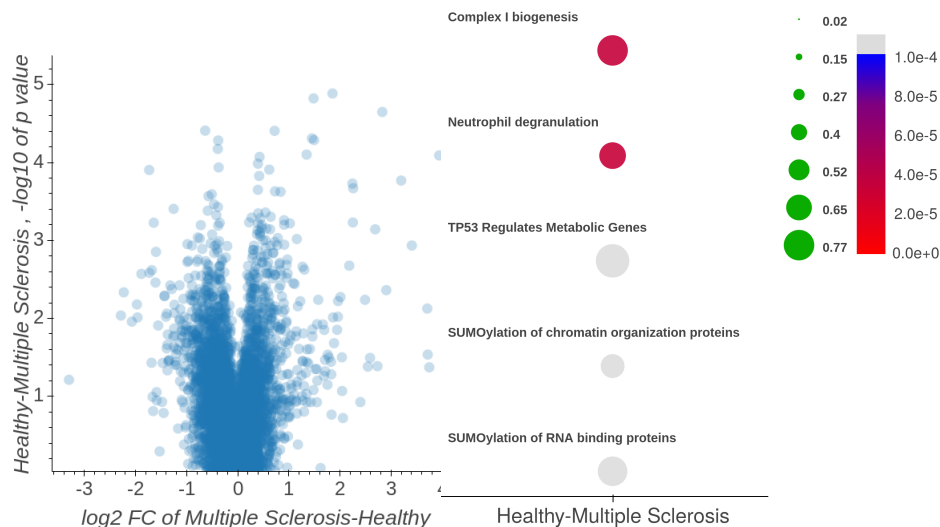
(a) The EPLS transcript weight plane with weights coloured by alignment to MS state (b) The EPLS sample scores with samples coloured by MS state

Figure 2: EPLS model of the MS state.

significant weights in the same quadrants as samples. The  $\mathbf{Y}$  matrix, describing the **MS** and **Healthy** subjects sample score weights are also in the same quadrants. We can calculate the angular proximity between the sample score weights and the transcripts feature weights and assign what transcripts are closest to a particular score weight. This allows us to colour the transcripts according to the descriptor that best captures their variation in the data. We can also define new vectors corresponding to different directions on the transcript weight plane.

In Figure 3a, we depict the negative logarithm of the EPLS  $p$ -values on the  $y$ -axis and fold change values on the  $x$ -axis. In this case, the EPLS model describes the separation between **Healthy** and **MS** patients and the  $p$  values are thus analogue to  $t$ -test comparison based  $p$  values resulting in a volcano plot appearance. The axis describing the Healthy-Multiple Sclerosis state variation  $p$  values can then be employed to calculate pathway enrichments. In Figure 3b, the pathway enrichment has been calculated using a Fisher exact test together with the Reactome pathway database. For each pathway, significant genes are deduced based on a  $p$ -value cutoff equal to 0.05 and a contingency table is produced. The resulting contingency table is then evaluated using a two-sided Fisher exact test. We choose a two-sided test because we employ a variational model. As such the enrichment does not correspond to an up or down-regulated accumulation in the group but rather correspond to if the group is important in describing the EPLS axis.

In Figure 4 we study the gene associations calculated directly from the EPLS feature weights. The feature associations can be calculated from the angle between two transcripts,  $\beta$ , on the transcript EPLS weight plane. All pairs of  $\cos(\beta)$  make up an association map for the EPLS model. The values range from +1, for fully aligned, through 0, for orthogonal, to -1 for antialigned. The EPLS solution constructs a model surface that maximizes the variance between the  $\mathbf{Y}$  axes. This is the reason



(a) The gene transcripts associated with EPLS  $p$  values against  $\log_2$  fold changes. (b) Hierarchically corrected pathway enrichment.

Figure 3: Sizes corresponds to gene ratios and the significance levels depicted are raw  $p$  values.

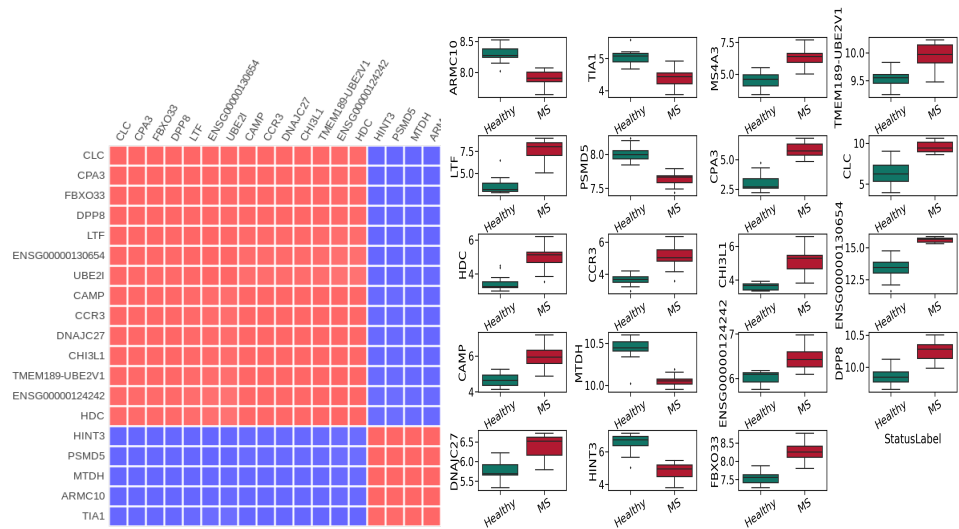
why the association map represents an over accentuated correlation map of the genes depicted.

By selecting a smaller subset of transcripts, here with  $q < 0.16$  values, and calculating the association map we see that the significant transcripts are roughly divided into two anti-associated clusters. Under the assumption that our coding genes produce proteins, we may utilize `string-db` [9] to analyse them. We find that they enrich for immune system activity in the specific and tertiary granule lumens. The largest cluster enriches for antifungal humoral response and innate immune response in mucosa while the second cluster enriches for publications on long non-coding RNA activity. In the second cluster, the gene with the highest intersection among such publications is the `PSMD5` transcript. The protein of this gene has also been reported for proteomic quantification of differentially expressed genes between `MS` and `Healthy` patients [23].

From Figure 5a it is clear that our EPLS model derived  $p$ -values are conservative estimates when compared to those stemming from a t-test. From Figure 5b it is clear that the  $p$ -value distribution is heteroscedastic around the  $y \approx 0.5x$  line in the logarithmic  $p$ -value space numerically proving that we are quantifying the same type of discoveries as the t-test, but with much more conservative estimates of the  $p$ -values.

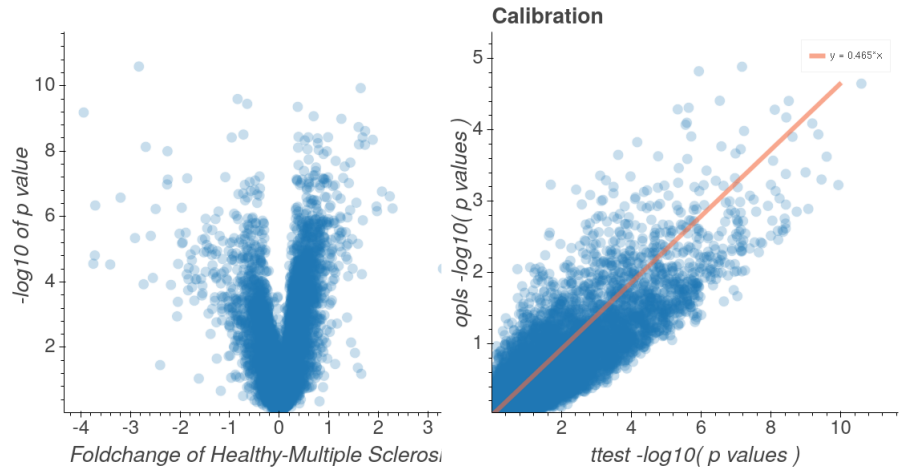
### 3.2 TCGA-BRCA and the comparison with a two-way ANOVA

In this section we study the TCGA Breast cancer dataset [24] under EPLS and a type-2 ANOVA. Clinical parameters [25], as well as messenger Ribonucleic Acid (mRNA)



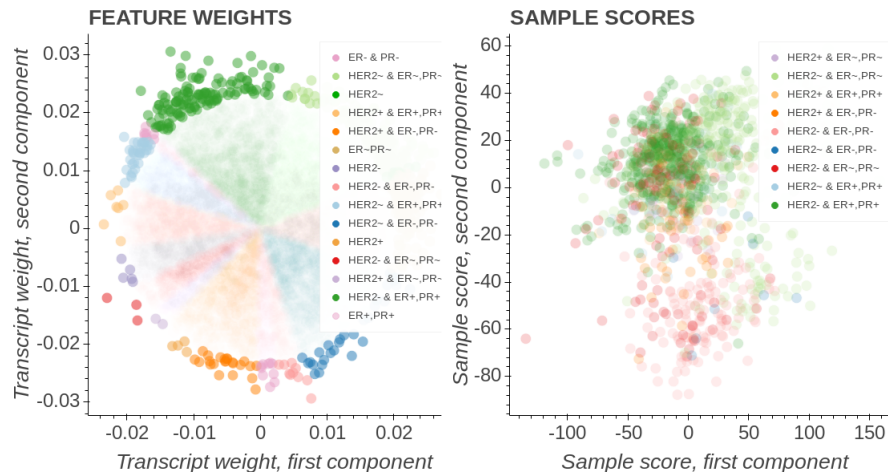
(a) The gene transcripts association map. Colors correspond to the cosine of the angle between the feature weights. (b) Quantification of the transcripts with most significant group differences.

Figure 4: Gene transcription association exploration.



(a) Volcano plot with ttest  $p$ -values plotted against  $\log_2$  fold changes. (b) Comparison of the our model  $p$ -values and traditional t-test derived  $p$ -values.

Figure 5: MS Comparison of opls and t-test produced  $p$ -values.



(a) Transcript weight colored by their hormone alignment owners. (b) The sample scores show that triple negative patients are diametrically opposed to **HER2-** & **PR+**, **ER+** patients.

Figure 6: EPLS model of the TCGA breast cancer data set.

expression data from human female patients. These were obtained from the TCGA website [24]. All of the downloaded samples originated from Illumina RNA-Seq data using the High Throughput Sequencing (HTS) 3 FPKM workflow [26]. In the case where more than one expression profile belonged to one sample id we randomly selected one of the profiles. Sample receptor statuses [27] were stored as **ER+**, **ER-**, **PR+**, **PR-**, **HER2+**, **HER2-** or **ND** in a sample journal file. This resulted in 1184 breast cancer samples [21].

In Figure 6 we employed an EPLS model of the form

$$\text{Transcript} \sim C(\text{HER2}) : C(\text{ERPR}) + C(\text{HER2}) + C(\text{ERPR})$$

and coloured all the group instances with unique colours. The **HER2** group describes the **HER2** receptor state while the Estrogen Receptor Progesterone Receptor (**ERPR**) group describes whether or not the **ER** and **PR** receptors are in a particular state. Thus triple-negative patients will belong to the **HER2-** & **PR-**, **ER-** intergenetion and triple positive to the **HER2+** & **PR+**, **ER+**. It is well known that triple-negative patients have a poor survival outcome for breast cancer and are interesting to study in this context. Figure 6b shows that triple-negative patients amass in the most southern parts of the lower quadrants. Diametrically opposed we find the patients bearing the interaction combination belonging to **HER2-** & **PR+**, **ER+**. We note that the triple-positive group form an angle of roughly 110 degrees to the triple-negative group. From here on we call the triple-negative towards **HER2-**, **PR+**, **ER+** axis the high-risk axis.

Among the genes with the strongest association to the high-risk axis, we find **ESR1**, **CXXC5**, **GREB1**, **FOXA1** and **GATA3**. They enrich [9] for estrogen-dependent gene expression in Reactome as well as the prostate gland and uterus development in biological processes [12]. We only have women in the data so we safely assume that the prostate

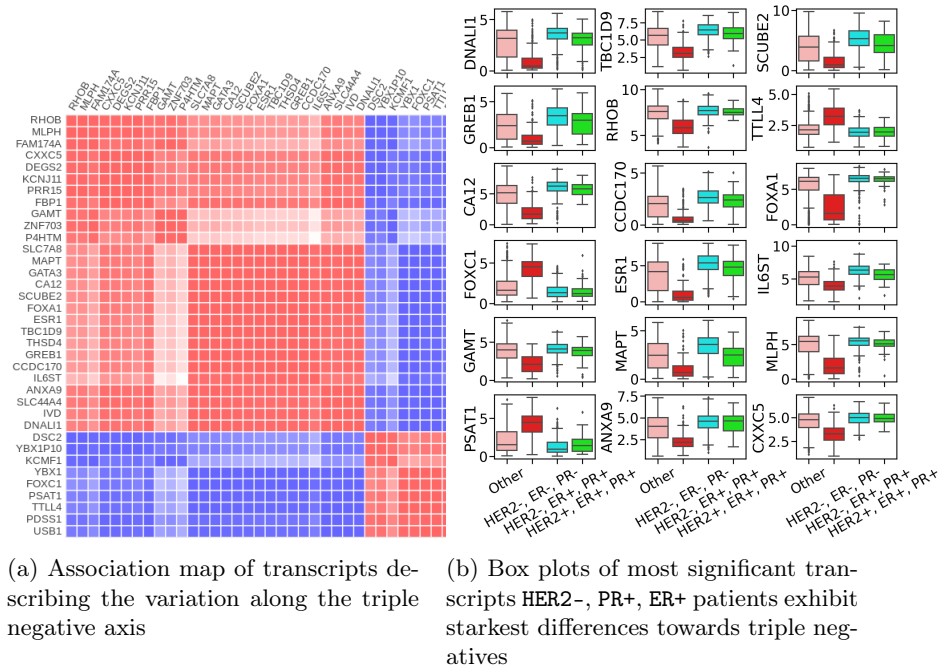


Figure 7: EPLS model association map of the TCGA breast cancer data set.

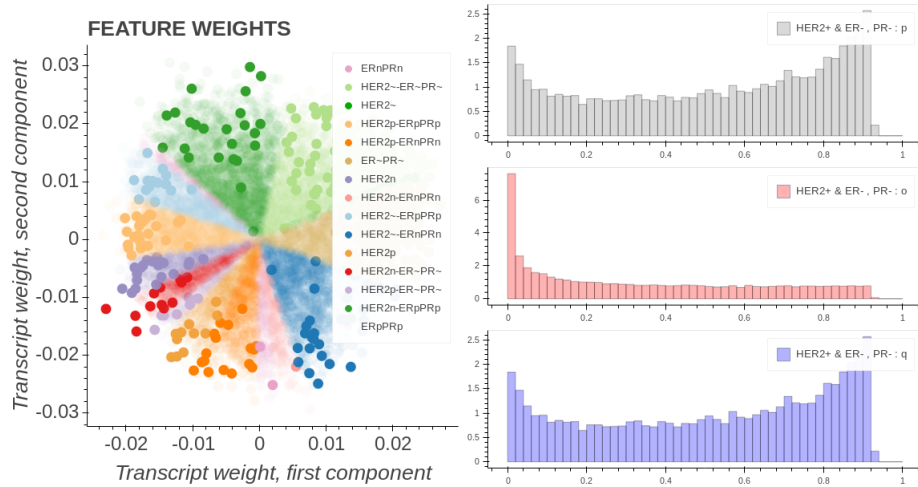
gland enrichment is due to the interaction of these genes with the progesterone receptor in men.

In Figure 7b, we find the traditional quantification of the transcript data. Triple-negative patients are remarkably different from the other groups. We also show both triple-positive as well as HER2-, PR+ and ER+ patient groupings. The EPLS model in Figure 6b conveyed the information that HER2-, PR+, ER+ combination are anti associated to the triple negatives and we can also see that the biggest difference in the boxplots of Figure 7b is found between the triple-negative and HER2-, PR+, ER+ group. It is also becomes apparent that the gene cluster associated with being up in triple-negative patients belong to PSAT1, TTL4, FOXC1, USB1, PDSS1, YBX1, KCMF1, YBX1P10 and DSC2. It constitutes a novel cluster for describing triple-negative patients and it is only when evaluated along the high-risk axis that the full picture emerges.

These results would not be complete without mentioning the statistical properties of the weights. Since there is no warranty that EPLS models converge on any specific residual distribution this can become convoluted. The maximisation of variance on the common subspace plane implies that a solution would minimize the EPLS models squared residual. In using our formalism we can study the same formula using both an ANOVA as well as an EPLS model. In Figure 8b we show the same statistical model,

$$\text{Transcript} \sim C(\text{HER2}) : C(\text{ERPR}) + C(\text{HER2}) + C(\text{ERPR})$$

produces qualitatively similar results.



(a) The  $p$  values produced by the EPLS model as well as the intermittent  $o$  and final two-way ANOVA  $q < \frac{0.05}{10455}$  shown with full opacity. (b) EPLS model with all transcripts having  $q < \frac{0.05}{10455}$  shown with full opacity.

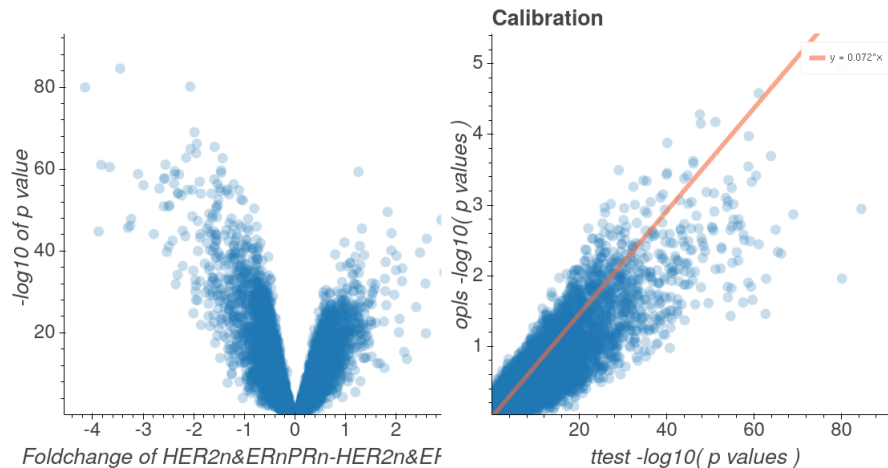
In Figure 8a depicts the EPLS model where all the interaction categories of

$$\text{Transcript} \sim C(\text{HER2}) : C(\text{ERPR})$$

are shown. The transcripts are also modelled using a two-way ANOVA and all transcripts having an interaction with a  $q < \frac{0.05}{10455}$  are depicted in full opacity. Two realizations are immediate. The first is that the ANOVA results are qualitatively similar to those of the EPLS, with a large density of significant ANOVA transcripts being found on the rim of the EPLS weight plane. Our EPLS model, however, offers an improvement in that we may determine not just the specific interaction pair associated with which transcript but also the direction. From our model, we can recognize that *TTL4* will be scaling in magnitude with the triple-negative state as well as being significantly different from the other groupings. The traditional box plot quantification in Figure 7b is important but not essential. We further explore our EPLS  $p$ -values and it is clear from Figure 8a that we have a large accumulation of weights near the centre. This also means that we are more prone to false discoveries near the centre. One can directly correct for this in the  $q$  value calculation by assuming that the False Discovery Rate (FDR) scale linearly with the Fractional Rank (FR) of the list of  $p$  values, which is quantified by:

$$\text{fr}(p) = \frac{\text{ranks}(p)}{\text{length}(p)}$$

Instead of assuming a constant FDR [28] across  $p$  values, often set equal to 1, for the  $q$  value calculation we set it to scale using the FR formula. These scaled  $p$  values are here dubbed  $o$  values and are only used to show the effect of this scaling. The final  $q$  values are showed in Figure 8b. We recognize that the EPLS transcripts with significant interaction all belong to the rim of the categories defined by the axis studied (here the far edge of the *HER2+*, *PR-*, *ER-* axis).



(a) Volcano plot with ttest  $p$ -values plotted against  $\log_2$  fold changes. (b) Comparison of the our model  $p$ -values and traditional t-test derived  $p$ -values.

Figure 9: TCGA Comparison of EPLS and t-test produced  $p$ -values.

By inspecting Figure 9 we can see that the axis found also generates the high significance interaction using a t-test. One could numerically perform all pairwise t-tests, we will refrain from doing, in order to draw a conclusion about whether this axis has the highest t-test significance. Instead we note that, from Figure 6a, the axis grouping containing the triple negative samples as well as their diametrically opposed group is the  $\text{HER2-}\&\text{ER-},\text{PR-}$   $\text{HER2-}\&\text{ER+},\text{PR+}$  pair and not the triple positive group. The t-test significance magnitude drops to half of that obtained from the axis reported as the most important axis when changed to triple negatives paired against triple positives. From Figure 9b the method remains heteroscedastic around a power law relation. However here our  $p$ -values roughly fall on the  $y \approx x * 0.072$  line in log space. As such we remain conservative in our  $p$ -value quantification with respect to a t-test along a comparable axis. In this case our  $p$ -values are still of the same order of magnitude as in Figure 5a. This is due to the fact that they are computed from the transcript position and the transcript density. Since this is decoupled from the samples in the EPLS model we can evaluate it across an arbitrary attribute axis. The transcript density is defined by roughly the same amount of transcripts in the Multiple Sclerosis and Breast Cancer cases and the transcript  $p$ -value magnitudes is therefore comparable and of the same order of magnitude for both of the EPLS models. The EPLS weight alignment become more reliable as more samples are added but this information is not directly conveyed to the EPLS  $p$ -values. We note that, as in Figure 5b, that our  $p$ -values are conservative. By noting that we are projecting onto a spherical solution space (2-dimensional) where the opls axis (1-dimensional) is set by the sample space we realize that our axis  $p$ -values will calibrate towards t-test derived  $p$ -values, across the same sample grouping axis as in equation 1

$$p_{\text{opls,axis}} \approx p_{\text{t-test,axis}} \sqrt{\frac{N_{\text{samples}}}{2\pi}} \quad (1)$$

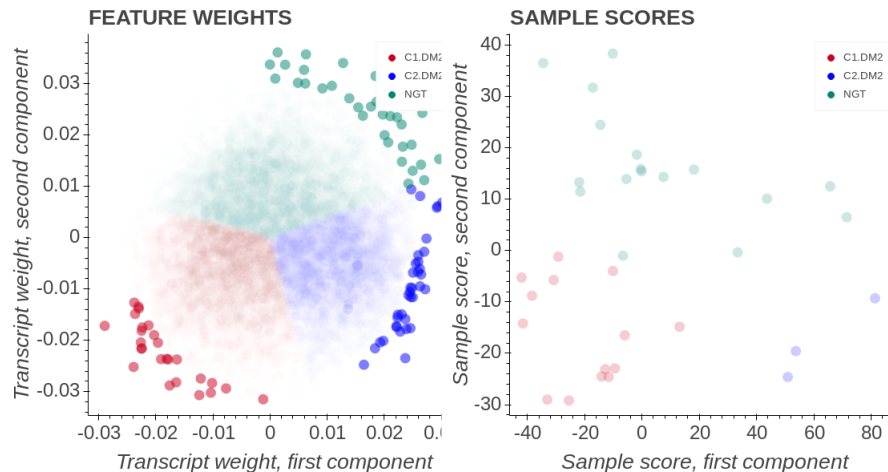


Figure 10: T2D & NGT EPLS model with all transcripts.

The main advantage of our method is that we can, using an unbiased method, identify the group that is diametrically opposed to the disease group.

### 3.3 Diabetes Microarray Analysis

Type 2 Diabetes is a metabolic disease on the rise in the general populous. It is furthermore influenced by both lifestyle choices as well as genetic factors. Understanding the detailed balance required for this disease phenotype to emerge is important to achieve better therapies and quality of life of those affected by it. The understanding of altered metabolism is also of great importance since many diseases are associated with altered cell and tissue metabolism [29].

There is an increasing amount of evidence that type 2 diabetes T2D, or Diabetes Mellitus 2 (DM2), disease phenotype constitutes several underlying metabolic disease phenotypes [30].

Here we have chosen to study human DM2 data from the Broad Institute [29]. Suspecting that we have more than a single type of DM2 patients we first segmented the data. This was done by employing approximative density clustering as implemented in our package [19]. Because of the limited number of samples (18) we stopped once we had obtained the two most separated sample groups. We thereby obtain two well-separated DM2 cluster types that we name C1.DM2 and C2.DM2 where the cluster index is the inverted cluster size rank.

In Figure 10 we see that the second cluster consists of only three samples. They form a group well-separated from the rest but lying close to orthogonal to the Normal Glucose Tolerance (NGT) group. The first cluster forms an axis with the NGT group with weights being positioned opposed to one another. Using our EPLS model we would believe that they constitute a smaller DM2 phenotype subset with distinct metabolic alterations. By studying the  $p$ -values associations on the rim of the entire EPLS graph we find that *FAM35A* have  $q < \frac{0.05}{N_{transcripts}}$  and aligning with the C1.DM2



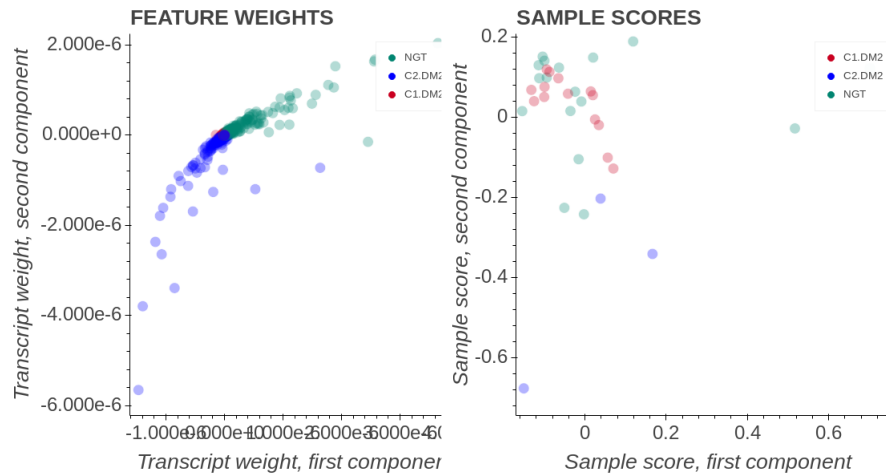


Figure 12: T2D & NGT PCA model with all transcripts.

when employing PCA.

## 4 Discussion

It should be noted that the method is meant to be used as an exploratory descriptive method. There has been no attempt to validate its efficacy for inference. KNN is also a method that can be implemented in multiple ways and in this specific case 1-NN was employed simply because the PLS operations are taken beforehand, ostensibly removing noise from each “centroid”.

An alternate way of studying  $Y$  space variance would be via discriminant analysis, as suggested by research related to [13] and [33]. OPLS-DA solves this but cannot relate a specific feature to a specific attribute.

Leaving the general discussion aside we also have comments regarding the use case specific results in the following three subsections. These discussions are to elaborate on the suitability of the method uncovered results.

### 4.1 Multiple Sclerosis

Regarding the multiple sclerosis use case we see from Figure 3 in Section 3.1 that the major pathways deduced are complex I biogenesis and neutrophil granulation, pathways which are affiliated with increased metabolism and immune system activity. Compartment enrichment analysis, also utilizing a two-sided Fisher exact test, of our  $p$ -values tells us that the dataset is mainly active in the cytosol, nucleoplasm and ficolin-1-rich granule membrane. This conveys the picture that we are dealing with neutrophil degranulation and metabolism of surface membranes. This is aligned with the common view that MS is associated with demyelination of axon myelin. Roughly translating into altered lipid metabolism by the immune system.

Our modelling scheme shows weaker statistical power than other methods but recovers fundamental and broad descriptive knowledge about the dataset. We also identify a small subset of significant genes that are differentially expressed in the cohort and share an intersection with proteomic analysis. Both the proteomic derived set as well as our EPLS transcriptome analysis does not share a large common intersecting set with the differentially expressed genes published together with the Genome Wide Association Study (GWAS) dataset that we employed. This analysis method should as such be viewed as a complementary method for producing a data-driven story of the cohort as well as targets of interest for use in further biological validation. In this section, we have shown how the  $\mathbf{Y}$  matrix alignments translate into the feature space of EPLS models.

Looking at Figure 4a and allowing ourself down into the first 100 significant EPLS genes, with a  $p < 0.0002$  value, we see a common intersection set between our results and the [23] proteins. These are **TES**, **CLTC**, **SIN3A** as well as **PSMD5** and known to influence **RUNX1** transcription pathways.

## 4.2 Breast Cancer

In the breast cancer use case; the Forkhead box (FOX) C1 transcript is thought to be a possible target in nasopharyngeal carcinoma [34]. **FOXA1** is similarly known to be correlated with **GATA3**, Progesteron receptor protein expression and clinical outcomes in breast cancer [27] as well as prostate cancer [35]. However, some of the associations in Figure 7a are new and might be interesting targets for further biological validation. It is worth further emphasis that these gene transcripts correspond to the outliers lying on the axis connecting the triple-negative and the **HER2-**, **PR+**, **ER+** in the EPLS feature weight plane.

One can compare the association map in Figure 7 to an alternate method, such as a clustered correlation heatmap. In Figure 13 we can see a clustermap providing the qualitative same results, while residing on a fundamentally different mathematical approach. Meaning that obtaining a gene cosine angle value close to 1 will obtain a rank correlation close to 1 and that, similarly, anti-aligned genes become anti-correlated.

## 4.3 Type 2 Diabetes

Hierarchical modelling or agglomerative hierarchical clustering are well-known methods of partitioning one's data. Traditionally, building hierarchical models are done via curating knowledge and manually constructing a hierarchy [11, 30]. One can also choose to computationally construct hierarchical data structures using agglomerative hierarchical clustering [36] or simply try to find the grouping that will separate the density the most [19].

Guided by Figure 11 we see an enrichment [9] for Guanosine TriPhosphate (GTP) metabolism in the mitochondria. We know that mitochondrial GTP metabolism is essential for glucose-dependent insulin secretion [37]. It is known that this will lead to disrupted oxidative phosphorylation and an altered mitochondrial membrane potential [36]. Furthermore, mitochondria maintain oxidative phosphorylation by creating a membrane potential, also implying an altered membrane potential will lead to altered oxidative phosphorylation [38]. This together is indicative that Adenosine TriPhosphate (ATP) synthesis might be inhibited, for the diabetics, in the mitochondria [39]. These findings are qualitatively similar to those reported by [29]. This is indeed good

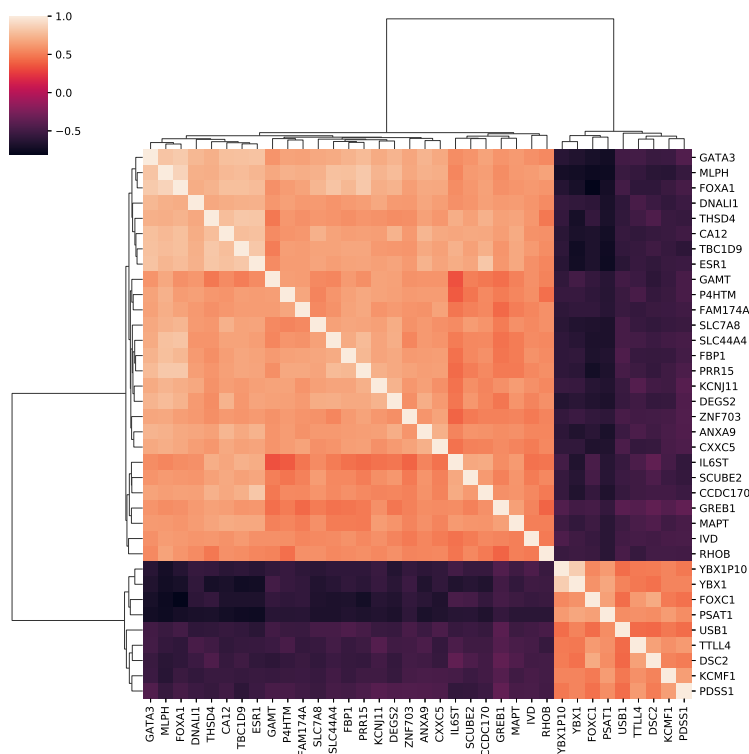


Figure 13: Clustered correlation heatmap of the genes identified by the EPLS method for the triple-negative axis.

news since we are studying people whom, by definition, have inhibited metabolic regulatory control of glucose and insulin.

## 5 Conclusions

We have developed a new analysis method and code library, as described in Section 2 and 2.1, for use in bioinformatic analysis. We have demonstrated the use of EPLS models for transcriptomic analysis on three different mRNA data sets, MS (Section 3.1), TCGA-BRCA (Section 3.2) and T2D (Section 3.3).

Our models produce unbiased sensible descriptions of the endpoint endogen states where we can relate what we see in the data to known properties of the human patient samples that we studied, as discussed in Section 4. We can see that PLS, through clever encoding and alignment produces sample attribute specific insights. We have shown how the alignment of the sample to feature scores translate into the ability to interpret feature weights in the context of the sample weights. As such the realization that the weights of the feature and sample descriptor matrices are aligned facilitates the use of the feature weights directly in traditional pathway analysis methods. This

also means that a high weight in the direction of a predictor axis will equate to large, between-group, difference quantifications lying on that axis. In contrast to, e.g. DSeq2 we can compare more than two known covariates against each other in a many to many comparison.

From this, several new and sensible interpretations of the data emerge. We can also confirm previously known properties of the samples. We find a gene cluster which follows the triple-negative breast cancer patients which have interesting suggestion targets for continued validation.

OPLS models are employed in such diverse research fields as financial forecasting [40], brain imaging [41] as well as environmental spatial characterization and forecasting [42].

We believe, as such, that this method is suitable as decision support for providing global suggestions of future study in high entropy domains.

To our knowledge, looking at other OPLS model applications, no one explores the orientation, or vector alignment, properties of such models.

## References

- [1] Wold S, Albano C, Dunn WJ, Edlund U, Esbensen K, Geladi P, Hellberg S, Johansson E, Lindberg W, Sjöström M. 1984 Multivariate Data Analysis in Chemistry. In Kowalski BR, editor, *Chemometrics: Mathematics and Statistics in Chemistry*, pp. 17–95. Dordrecht: Springer Netherlands.
- [2] Wegelin JA. 2000 A Survey of Partial Least Squares (PLS) Methods, with Emphasis on the Two-Block Case. .
- [3] Rothenberg DO, Yang H, Chen M, Zhang W, Zhang L. 2019 Metabolome and Transcriptome Sequencing Analysis Reveals Anthocyanin Metabolism in Pink Flowers of Anthocyanin-Rich Tea (*Camellia Sinensis*). *Molecules* **24**.
- [4] Eriksson L, Byrne T, Johansson E, Trygg J, Vikström C. 2013 *Multi- and Megavariate Data Analysis Basic Principles and Applications, Third Revised Edition*. Umetrics Academy.
- [5] Abdi H, Williams LJ. 2010 Principal Component Analysis: Principal Component Analysis. *Wiley Interdisciplinary Reviews: Computational Statistics* **2**, 433–459.
- [6] Rosipal R, Krämer N. 2006 Overview and Recent Advances in Partial Least Squares. In Saunders C, Grobelnik M, Gunn S, Shawe-Taylor J, editors, *Subspace, Latent Structure and Feature Selection* pp. 34–51 Berlin, Heidelberg. Springer Berlin Heidelberg.
- [7] Fisher RA. 1919 XV.—The Correlation between Relatives on the Supposition of Mendelian Inheritance.. *Transactions of the Royal Society of Edinburgh* **52**, 399–433.
- [8] Tapp HS, Kemsley EK. 2009 Notes on the Practical Utility of OPLS. *TrAC Trends in Analytical Chemistry* **28**, 1322–1327.
- [9] Szklarczyk D, Gable AL, Lyon D, Junge A, Wyder S, Huerta-Cepas J, Simonovic M, Doncheva NT, Morris JH, Bork P, Jensen LJ, von Mering C. 2019 STRING V11: Protein-Protein Association Networks with Increased Coverage, Supporting Functional Discovery in Genome-Wide Experimental Datasets.. *Nucleic acids research* **47**, D607–D613.
- [10] Kanehisa M, Goto S. 2000 KEGG: Kyoto Encyclopedia of Genes and Genomes. *Nucleic Acids Research* **28**, 27–30.
- [11] Jassal B, Matthews L, Viteri G, Gong C, Lorente P, Fabregat A, Sidiropoulos K, Cook J, Gillespie M, Haw R, Loney F, May B, Milacic M, Rothfels K, Sevilla C, Shamovsky V, Shorser S, Varusai T, Weiser J, Wu G, Stein L, Hermjakob H, D’Eustachio P. 2019 The Reactome Pathway Knowledgebase. *Nucleic Acids Research*.
- [12] Mi H, Muruganujan A, Ebert D, Huang X, Thomas PD. 2018 PANTHER Version 14: More Genomes, a New PANTHER GO-Slim and Improvements in Enrichment Analysis Tools. *Nucleic Acids Research* **47**, D419–D426.
- [13] Trygg J, Wold S. 2002 Orthogonal Projections to Latent Structures (O-PLS). *Journal of Chemometrics* **16**, 119–128.
- [14] Alexa A, Rahnenfuhrer J, Lengauer T. 2006 Improved Scoring of Functional Groups from Gene Expression Data by Decorrelating GO Graph Structure. *Bioinformatics* **22**, 1600–1607.

- [15] Pedregosa F, Varoquaux G, Gramfort A, Michel V, Thirion B, Grisel O, Blondel M, Prettenhofer P, Weiss R, Dubourg V, Vanderplas J, Passos A, Cournapeau D, Brucher M, Perrot M, Duchesnay E. 2011 Scikit-Learn: Machine Learning in Python. *Journal of Machine Learning Research* **12**, 2825–2830.
- [16] Geladi P, Kowalski BR. 1986 Partial Least-Squares Regression: A Tutorial. *Analytica Chimica Acta* **185**, 1–17.
- [17] Höskuldsson A. 1988 PLS Regression Methods. *Journal of Chemometrics* **2**, 211–228.
- [18] Tjörnhammar E, Tjörnhammar R. 2020 Exploratory Projection to Latent Structure Models for Use in Transcriptomic Analysis, Experiment Code. .
- [19] Tjörnhammar R. 2019 Impetuous-Gfa. .
- [20] Seabold S, Perktold J. 2010 Statsmodels: Econometric and Statistical Modeling with Python. In *9th Python in Science Conference*.
- [21] Tjörnhammar R. 2019 MS and TCGA Dataset. .
- [22] Kempainen AK, Kaprio J, Palotie A, Saarela J. 2011 Systematic Review of Genome-Wide Expression Studies in Multiple Sclerosis. *BMJ Open* **1**.
- [23] Berge T, Eriksson A, Brorson IS, Høgestøl EA, Berg-Hansen P, Døskeland A, Mjaavatten O, Bos SD, Harbo HF, Berven F. 2019 Quantitative Proteomic Analyses of CD4(+) and CD8(+) T Cells Reveal Differentially Expressed Proteins in Multiple Sclerosis Patients and Healthy Controls. *Clinical proteomics* **16**, 19–19.
- [24] Koboldt DC, Fulton RS, McLellan MD, Schmidt H, Kalicki-Veizer J, McMichael JF, Fulton LL, Dooling DJ, Ding L, Mardis ER, Wilson RK, Ally A, Balasundaram M, Butterfield YSN, Carlsen R, Carter C, Chu A, Chuah E, Chun HJE, Coope RJN, Dhalla N, Guin R, Hirst C, Hirst M, Holt RA, Lee D, Li HI, Mayo M, Moore RA, Mungall AJ, Pleasance E, Gordon Robertson A, Schein JE, Shafiei A, Sipahimalani P, Slobodan JR, Stoll D, Tam A, Thiessen N, Varhol RJ, Wye N, Zeng T, Zhao Y, Birol I, Jones SJM, Marra MA, Cherniack AD, Saksena G, Onofrio RC, Pho NH, Carter SL, Schumacher SE, Tabak B, Hernandez B, Gentry J, Nguyen H, Crenshaw A, Ardlie K, Beroukhi R, Winckler W, Getz G, Gabriel SB, Meyerson M, Chin L, Park PJ, Kucherlapati R, Hoadley KA, Todd Auman J, Fan C, Turman YJ, Shi Y, Li L, Topal MD, He X, Chao HH, Prat A, Silva GO, Iglesia MD, Zhao W, Usary J, Berg JS, Adams M, Booker J, Wu J, Gulabani A, Bodenheimer T, Hoyle AP, Simons JV, Soloway MG, Mose LE, Jefferys SR, Balu S, Parker JS, Neil Hayes D, Perou CM, Malik S, Mahurkar S, Shen H, Weisenberger DJ, Triche Jr T, Lai PH, Bootwalla MS, Maglinte DT, Berman BP, Van Den Berg DJ, Baylin SB, Laird PW, Creighton CJ, Donehower LA, Getz G, Noble M, Voet D, Saksena G, Gehlenborg N, DiCara D, Zhang J, Zhang H, Wu CJ, Yingchun Liu S, Lawrence MS, Zou L, Sivachenko A, Lin P, Stojanov P, Jing R, Cho J, Sinha R, Park RW, Nazaire MD, Robinson J, Thorvaldsdottir H, Mesirov J, Park PJ, Chin L, Reynolds S, Kreisberg RB, Bernard B, Bressler R, Erkkila T, Lin J, Thorsson V, Zhang W, Shmulevich I, Ciriello G, Weinhold N, Schultz N, Gao J, Cerami E, Gross B, Jacobsen A, Sinha R, Arman Aksoy B, Antipin Y, Reva B, Shen R, Taylor BS, Ladanyi M, Sander C, Anur P, Spellman PT, Lu Y, Liu W, Verhaak RRG, Mills GB, Akbani R, Zhang N, Broom BM, Casavant TD, Wakefield C, Unruh AK, Baggerly K, Coombes K, Weinstein JN, Haussler D, Benz CC, Stuart JM, Benz SC, Zhu J, Szeto CC, Scott GK, Yau C, Paull EO, Carlin D, Wong C, Sokolov A, Thusberg J, Mooney S, Ng S,

- Goldstein TC, Ellrott K, Grifford M, Wilks C, Ma S, Craft B, Yan C, Hu Y, Meerzaman D, Gastier-Foster JM, Bowen J, Ramirez NC, Black AD, Pyatt RE, White P, Zmuda EJ, Frick J, Lichtenberg TM, Brookens R, George MM, Gerken MA, Harper HA, Leraas KM, Wise LJ, Tabler TR, McAllister C, Barr T, Hart-Kothari M, Tarvin K, Saller C, Sandusky G, Mitchell C, Iacocca MV, Brown J, Rabeno B, Czerwinski C, Petrelli N, Dolzhansky O, Abramov M, Voronina O, Potapova O, Marks JR, Suchorska WM, Murawa D, Kycler W, Ibbs M, Korski K, Spychała A, Murawa P, Brzeziński JJ, Perz H, Łażniak R, Teresiak M, Tatka H, Leporowska E, Bogusz-Czerniewicz M, Malicki J, Mackiewicz A, Wiznerowicz M, Van Le X, Kohl B, Viet Tien N, Thorp R, Van Bang N, Sussman H, Duc Phu B, Hajek R, Phi Hung N, Viet The Phuong T, Quyet Thang H, Zaki Khan K, Penny R, Mallery D, Curley E, Shelton C, Yena P, Ingle JN, Couch FJ, Lingle WL, King TA, Maria Gonzalez-Angulo A, Mills GB, Dyer MD, Liu S, Meng X, Patangan M, The Cancer Genome Atlas Network, Genome sequencing centres: Washington University in St Louis, Genome characterization centres: BC Cancer Agency, Broad Institute, Brigham & Women’s Hospital & Harvard Medical School, University of North Carolina CH, University of Southern California/Johns Hopkins, Genome data analysis: Baylor College of Medicine, Institute for Systems Biology, Memorial Sloan-Kettering Cancer Center, Oregon Health & Science University, The University of Texas MD Anderson Cancer Center, University of California SCL, NCI, Biospecimen core resource: Nationwide Children’s Hospital Biospecimen Core Resource, Tissue source sites: ABS-IUPUI, Christiana, Cureline, Duke University Medical Center, The Greater Poland Cancer Centre, ILSBio, International Genomics Consortium, Mayo Clinic, MSKCC, MD Anderson Cancer Center. 2012 Comprehensive Molecular Portraits of Human Breast Tumours. *Nature* **490**, 61–70.
- [25] Tao M, Song T, Du W, Han S, Zuo C, Li Y, Wang Y, Yang Z. 2019 Classifying Breast Cancer Subtypes Using Multiple Kernel Learning Based on Omics Data.. *Genes* **10**.
- [26] Anders S, Pyl PT, Huber W. 2015 HTSeq—a Python Framework to Work with High-Throughput Sequencing Data. *Bioinformatics* **31**, 166–169.
- [27] Ross-Innes CS, Stark R, Teschendorff AE, Holmes KA, Ali HR, Dunning MJ, Brown GD, Gojis O, Ellis IO, Green AR, Ali S, Chin SF, Palmieri C, Caldas C, Carroll JS. 2012 Differential Oestrogen Receptor Binding Is Associated with Clinical Outcome in Breast Cancer. *Nature* **481**, 389–393.
- [28] Storey JD, Tibshirani R. 2003 Statistical Significance for Genomewide Studies. *Proceedings of the National Academy of Sciences* **100**, 9440–9445.
- [29] Mootha VK, Lindgren CM, Eriksson KF, Subramanian A, Sihag S, Lehar J, Puigserver P, Carlsson E, Ridderstråle M, Laurila E, Houstis N, Daly MJ, Patterson N, Mesirov JP, Golub TR, Tamayo P, Spiegelman B, Lander ES, Hirschhorn JN, Altshuler D, Groop LC. 2003 PGC-1 $\alpha$ -Responsive Genes Involved in Oxidative Phosphorylation Are Coordinately Downregulated in Human Diabetes. *Nature Genetics* **34**, 267–273.
- [30] Ahlqvist E, Storm P, Käräjämäki A, Martinell M, Dorkhan M, Carlsson A, Vikman P, Prasad RB, Aly DM, Almgren P, Wessman Y, Shaat N, Spégel P, Mulder H, Lindholm E, Melander O, Hansson O, Malmqvist U, Lernmark Å, Lahti K, Forsén T, Tuomi T, Rosengren AH, Groop L. 2018 Novel Subgroups of Adult-Onset Diabetes and Their Association with Outcomes: A Data-Driven

- Cluster Analysis of Six Variables. *The Lancet Diabetes & Endocrinology* **6**, 361–369.
- [31] Uhlén M, Fagerberg L, Hallström BM, Lindskog C, Oksvold P, Mardinoglu A, Sivertsson Å, Kampf C, Sjöstedt E, Asplund A, Olsson I, Edlund K, Lundberg E, Navani S, Szigartyo CAK, Odeberg J, Djureinovic D, Takanen JO, Hober S, Alm T, Edqvist PH, Berling H, Tegel H, Mulder J, Rockberg J, Nilsson P, Schwenk JM, Hamsten M, von Feilitzen K, Forsberg M, Persson L, Johansson F, Zwahlen M, von Heijne G, Nielsen J, Pontén F. 2015 Tissue-Based Map of the Human Proteome. *Science* **347**, 1260419.
- [32] Galderisi U, Jori FP, Giordano A. 2003 Cell Cycle Regulation and Neural Differentiation. *Oncogene* **22**, 5208–5219.
- [33] Wold H. 2006 Partial Least Squares. In *Encyclopedia of Statistical Sciences* , . American Cancer Society.
- [34] Ou-Yang L, Xiao SJ, Liu P, Yi SJ, Zhang XL, Ou-Yang S, Tan SK. 2015 Forkhead Box C1 Induces Epithelial-mesenchymal Transition and Is a Potential Therapeutic Target in Nasopharyngeal Carcinoma.. *Molecular Medicine Reports* **12**, 8003–8009.
- [35] Barbieri CE, Baca SC, Lawrence MS, Demichelis F, Blattner M, Theurillat JP, White TA, Stojanov P, Van Allen E, Stransky N, Nickerson E, Chae SS, Boysen G, Auclair D, Onofrio RC, Park K, Kitabayashi N, MacDonald TY, Sheikh K, Vuong T, Guiducci C, Cibulskis K, Sivachenko A, Carter SL, Saksena G, Voet D, Hussain WM, Ramos AH, Winckler W, Redman MC, Ardlie K, Tewari AK, Mosquera JM, Rupp N, Wild PJ, Moch H, Morrissey C, Nelson PS, Kantoff PW, Gabriel SB, Golub TR, Meyerson M, Lander ES, Getz G, Rubin MA, Garraway LA. 2012 Exome Sequencing Identifies Recurrent SPOP, FOXA1 and MED12 Mutations in Prostate Cancer. *Nature Genetics* **44**, 685–689.
- [36] Mehta P, Bukov M, Wang CH, Day AG, Richardson C, Fisher CK, Schwab DJ. 2019 A High-Bias, Low-Variance Introduction to Machine Learning for Physicists. *A high-bias, low-variance introduction to Machine Learning for physicists* **810**, 1–124.
- [37] Kibbey RG, Pongratz RL, Romanelli AJ, Wollheim CB, Cline GW, Shulman GI. 2007 Mitochondrial GTP Regulates Glucose-Stimulated Insulin Secretion. *Cell Metabolism* **5**, 253–264.
- [38] Momcilovic M, Jones A, Bailey ST, Waldmann CM, Li R, Lee JT, Abdelhady G, Gomez A, Holloway T, Schmid E, Stout D, Fishbein MC, Stiles L, Dabir DV, Dubinett SM, Christofk H, Shirihai O, Koehler CM, Sadeghi S, Shackelford DB. 2019 In Vivo Imaging of Mitochondrial Membrane Potential in Non-Small-Cell Lung Cancer. *Nature* **575**, 380–384.
- [39] Sivitz WI, Yorek MA. 2010 Mitochondrial Dysfunction in Diabetes: From Molecular Mechanisms to Functional Significance and Therapeutic Opportunities. *Antioxidants & redox signaling* **12**, 537–577.
- [40] Huang SC, Wu TK. 2010 Integrating Recurrent SOM with Wavelet-Based Kernel Partial Least Square Regressions for Financial Forecasting. *Expert Systems with Applications* **37**, 5698–5705.
- [41] Abdi H. 2010 Partial Least Squares Regression and Projection on Latent Structure Regression (PLS Regression): PLS REGRESSION. *Wiley Interdisciplinary Reviews: Computational Statistics* **2**, 97–106.

- [42] Thioulouse J, Chessel D, Champely S. 1995 Multivariate Analysis of Spatial Patterns: A Unified Approach to Local and Global Structures. *Environmental and Ecological Statistics* **2**, 1–14.